scientific reports



OPEN

The nanosized structure and relative paramagnetic properties of ZnFe₂O₄ by the polyol processes and the heat treatment processes

Le Hong Phuc¹, Yong Yang², Nguyen Thi Nhat Hang³, Nguyen Quan Hien¹, Ho Van Cuu⁴, Nguyen Huu Tri⁴, Nguyen Xuan Hoang⁵, Masayuki Nogami⁶ & Nguyen Viet Long⁴⊠

The controlled synthesis and paramagnetic properties of nanosized Zn–Fe–O oxides have been researched by the polyol and the heat treatment processes designed according to drying, annealing, and sintering from low to high temperatures. The structural changes have led to change weak superparamagnetism of nanosized Zn–Fe–O oxides in the forms of hybrid nanosized ZnO/ZnFe₂O₄ oxides into paramagnetism of nanosized ZnFe₂O₄ when the as-prepared samples of both ZnO and ZnFe₂O₄ oxides were isothermally annealed and sintered from low temperature at about 60 °C to high temperature at 950 °C for 2 h during their structural phase transitions in all the measurements of x-ray diffraction (XRD), vibrating sample magnetometer (VSM), scanning electron microscopy (SEM) and SEM/energy dispersive X-ray spectroscopy (EDX) combined methods. Interestingly, it is experimentally confirmed that one original paramagnetic hysteresis consists of paramagnetic segments and closed curves. Both normal and abnormal paramagnetic properties of ZnFe₂O₄ were carefully investigated.

Keywords The polyol processes, Heat treatment processes, Sintering, ZnO, ZnFe₂O₄, Paramagnetism

In recent years, the synthesis, fabrication, structural characterization, and investigation of the physical properties of magnetic micro- and nanomaterials with spinel-type crystal structures have garnered significant attention. This growing interest arises from the fact that these materials exhibit unique physicochemical characteristics and tunable functionalities at the nanoscale, making them promising candidates for a wide range of advanced engineering and technological applications¹⁻⁴. Among them, zinc ferrite (ZnFe₂O₄) is well known to adopt a spinel-type crystal structure, which plays a crucial role in determining its magnetic and physicochemical properties 5,6. Consequently, ZnFe₂O₄ and related spinel ferrites have attracted increasing attention due to their versatile applications in electronics, telecommunications, magnetism, electromagnetics, catalysis, energy conversion and storage, as well as environmental remediation^{7–14}. To realize these applications, a wide range of chemical and physical synthesis techniques have been employed for the preparation of spinel-type ZnFe₂O₄ (AB₂O₄, a generalized original structure) and related ferrite oxides. These include sol-gel methods, coprecipitation, hydrothermal and solvothermal synthesis, combustion processes, as well as solid-state reactions, each offering distinct advantages in terms of particle size control, crystallinity, and morphology^{15–25}. To meet the growing demand for magnetic micro- and nanosized powders, researchers have developed polyol-based synthesis routes for Co-, Ni-, and Fe-based magnetic ferrites, as well as Sr- and Ba-based hexaferrites. These processes often utilize sodium borohydride (NaBH₄) or potassium borohydride (KBH₄) as reducing agents, followed by heat treatment, annealing, and sintering to achieve desired crystallinity and magnetic properties^{26–31}. The development of next-generation ferrites and hexaferrites is expected to be driven by the incorporation and doping of cobalt (Co) as a key functional element^{27,28}. Currently, polyol-based synthesis routes are widely recognized for their significant advantages and cost-effectiveness in the fabrication of magnetic nanoparticles. This is largely

¹Institute of Advanced Technology, Vietnam Academy of Science and Technology, 1B, TL 29 Street, An Phu Dong Ward, Quarter 1, Ho Chi Minh City 700000, Vietnam. ²State Key Laboratory of High-Performance Ceramics and Superfine Microstructures, Shanghai Institute of Ceramics, Chinese Academy of Sciences, 1295 Dingxi Road, Shanghai 200050, China. ³Institute of Applied Technology, Thu Dau Mot University, 6 Tran Van On, Phu Hoa Ward, Thu Dau Mot City 820000, Vietnam. ⁴Department of Engineering and Technology, Saigon University, 273 An Duong Vuong, District 5, Ho Chi Minh City 700000, Vietnam. ⁵Faculty of Information Technology, HUTECH University of Technology, 475A Dien Bien Phu Street, BinhThanh District, Ho Chi Minh City 700000, Vietnam. ⁶Nagoya Institute of Technology, Showa, Nagoya 466-8555, Japan. [∞]email: nguyenvietlong@sgu.edu.vn

attributed to the inherent limitations and the complexity associated with conventional chemical and physical methods. These polyol processes provide better control over particle size, morphology, and dispersion, thereby offering a promising alternative for the scalable production of magnetic nanomaterials^{27,28}. Moreover, the increasing popularity of polyol processes can be attributed to their inherent technological advantages, primarily arising from the superior solubility and effective dissolution of precursors in glycols, including ethylene glycol (EG), polyethylene glycol (PEG), and similar solvents. Furthermore, a wide range of nanosized ZnFe₂O₄ ferrites have found the applications in sensing and photocatalysis^{22,32,33}. In the near future, new and advanced electrode materials, utilizing nanosized mixed ferrites, are anticipated to play a significant role in applications related to environmental management, catalysis, energy storage, and the conversion, especially for next-generation batteries and capacitors^{34–49}. Therefore, the heating and firing technologies necessitate precise and optimal experimental conditions to effectively synthesize engineered nanosized magnetic powders.

In this study, nanosized Zn-Fe-O oxides, including ZnO and ZnFe₂O₄, were synthesized through polyol processes and heat treatment processes at low and intermediate temperatures ranging from 60 to 700 °C. Subsequently, the crystal structure of the Zn-Fe-O oxides was transformed into a single crystal structure of ZnFe₂O₄ through annealing and sintering at temperatures between 800 °C and 950 °C. Moreover, the structures and properties of the nanosized Zn-Fe-O oxides, including ZnO and ZnFe₂O₄, were determined using XRD, VSM, and SEM measurements, in accordance with the engineered processes. In addition, the paramagnetic properties of all samples of nanosized Zn-Fe-O oxides were also discussed and analyzed in detail. Specifically, it was found that the single crystal structure of ZnFe₂O₄ was formed at high temperatures of 800 °C, 900 °C, and 950 °C. Finally, the exciting zigzag paramagnetic properties of nanosized Franklinite ZnFe₂O₄ oxides were also addressed.

Experimental

In the typical polyol processes, precursor chemicals used for synthesis were FeCl₃ (0.0625 M) (China, AR, CAS:10025-77-1; characteristic: yellow-brown crystals. Readily deliquescent in air), ZnCl₂ (China, AR, CAS: 7646-85-7; characteristic: white powder or powder. Strongly hygroscopic), NaOH (0.0625 M) (China, AR, CAS: 1370-73-2; characteristic: white uniform granular or flaky solid), EG (China, AR, CAS: 107-21-1), PVP (0.375 M) (China, AR; or Sigma-Aldrich), NaBH₄ (China, AR, CAS: 16940-66-2; appearance: white powder) purchased from industrial chemicals, following laboratory and industrial manufacturing approach. In the experiments, FeCl₃ (0.0625 M) and ZnCl₂ (0.0625 M) can be used for synthesis (or FeCl₃ (0.0625 M) can be replaced by FeCl₂ (0.0625 M)) (or both FeCl₂ and FeCl₃ were used) according to the lab skills and experiences of the experimenters, and the designed polyol processes²⁷⁻³¹. We did not need to present the detailed experiment here. The key idea was that the molar ratio for chemical synthetic reaction between FeCl₃ and ZnCl₂ must be carefully adjusted in 2.0,^{30,31} in comparison with the original chemical equation for synthesis of Fe₃O₄ oxides by scientists^{40,41,44}. To investigate the kinds of as-prepared nanosized Zn–Fe–O oxides, the most typical samples selected were used, which were prepared by heat processes and isothermally heated from low to high temperatures in air.

The annealing temperature points used were at about 60, 100, 200, 300, 400, 500, 600, 650, 700, 800, 900, and 950 °C for preparing the magnetic powder samples in a period of 2 h. Additionally, XRD, SEM (SEM/EDX), and VSM measurements were performed at room temperature in order to determine the crystal structures and related magnetic properties, respectively. Typically, the features of magnetism and hysteresis loops of M-H of nanosized Zn–Fe–O oxide powders were measured using a VSM, EZ9 vibrating sample magnetometer (VSM, MicroSense, LLC Corporation, USA), and demagnetization field (Hc) in the range of – 1500 to +1500 Oe. The crystal structures of the as-prepared samples (magnetic Zn–Fe–O powder samples) were investigated using XRD from 5 to 80° (Empyrean PANalytical diffractometer, USA). In particle size analysis and image data, the as-prepared Zn–Fe–O oxide powders were primarily investigated using ultrahigh-resolution scanning electron microscopy (FESEM, S-4800, Japan) to study their sizes, shapes, and compositions. In addition, SEM (Tescan Mira, Czech Republic) was used with an FEG Schottky electron emission source combined with SEM imaging and live elemental composition analysis. The high resolution for imaging and EDX analysis was maintained to investigate the as-prepared nanosized Zn–Fe–O oxide powders.

Results and discussion

XRD: structure of nanosized ZnFe₂O₄ oxides

In X-ray diffraction, Fig. 1 shows the XRD diagrams of Zn-Fe-O oxides that were isothermally heated at different temperatures, providing sufficient detail for understanding their crystallization. In the range of annealing temperatures of 60-950 °C for the samples for 2 h, the identified crystal parameters of two phases of ZnO and ZnFe₂O₄ oxides in the as-prepared Zn-Fe-O oxides exhibited the values of 2θ (°) or Two-Theta (deg), d(Å), I(%), and a set of (hkl) planes, i.e. Miller indices in the typical diagrams of XRD. See supplementary data file (see supplementary Fig. S1 (XRD of all of samples)), and (supplementary Fig. S2 (XRD of ZnFe,O4 samples heated at 800, 900, and 950 °C, in respect with as-prepared samples in Figures: \$3, \$4, \$5, \$6, \$7, and S8)). It is emphasized that the XRD data and results of the as-prepared samples of the major phase of nanosized ZnFe₂O₄ oxides coincided with the standard pattern of PDF#74-2397, with 18 lines (Franklinite, syn, ZnFe₂O₄). cubic structure, Fd-3 m (227)) using λ radiation (CuK α 1, λ =1.5406Å) in the primary crystal characteristics. Therefore, the crystal phases of nanosized $ZnFe_2O_4$ oxides show the cubic structure in a cell (a, b, c (Å): 8.4432, 8.4432, 8.4432; α , β , γ (°): 90.0, 90.0, 90.0). All the samples show the 13 strong lines, and the strongest intensity, i.e. I(%) of (311) plane is 100% of intensity. The most typical values of 20 (18.184, 29.908, 35.225, 36.846, 42.806, 53.059, 56.595, 62.139, 65.330, 70.479, 73.488, 74.480, and 78.450 (°), respectively), d (4.8747, 2.9851, 2.5457, 2.4373, 2.1108, 1.7235, 1.6249, 1.4926, and 1.4272(Å), respectively), I(4.2, 32.2, 100, 7.6, 17.5, 14.9, 45.7, 55.9, 0.9, 5.7, 12.7, 5.2, and 2.7%, respectively), and the Miller index, i.e. a set of (hkl) ((111), (220), (311), (222), (400),

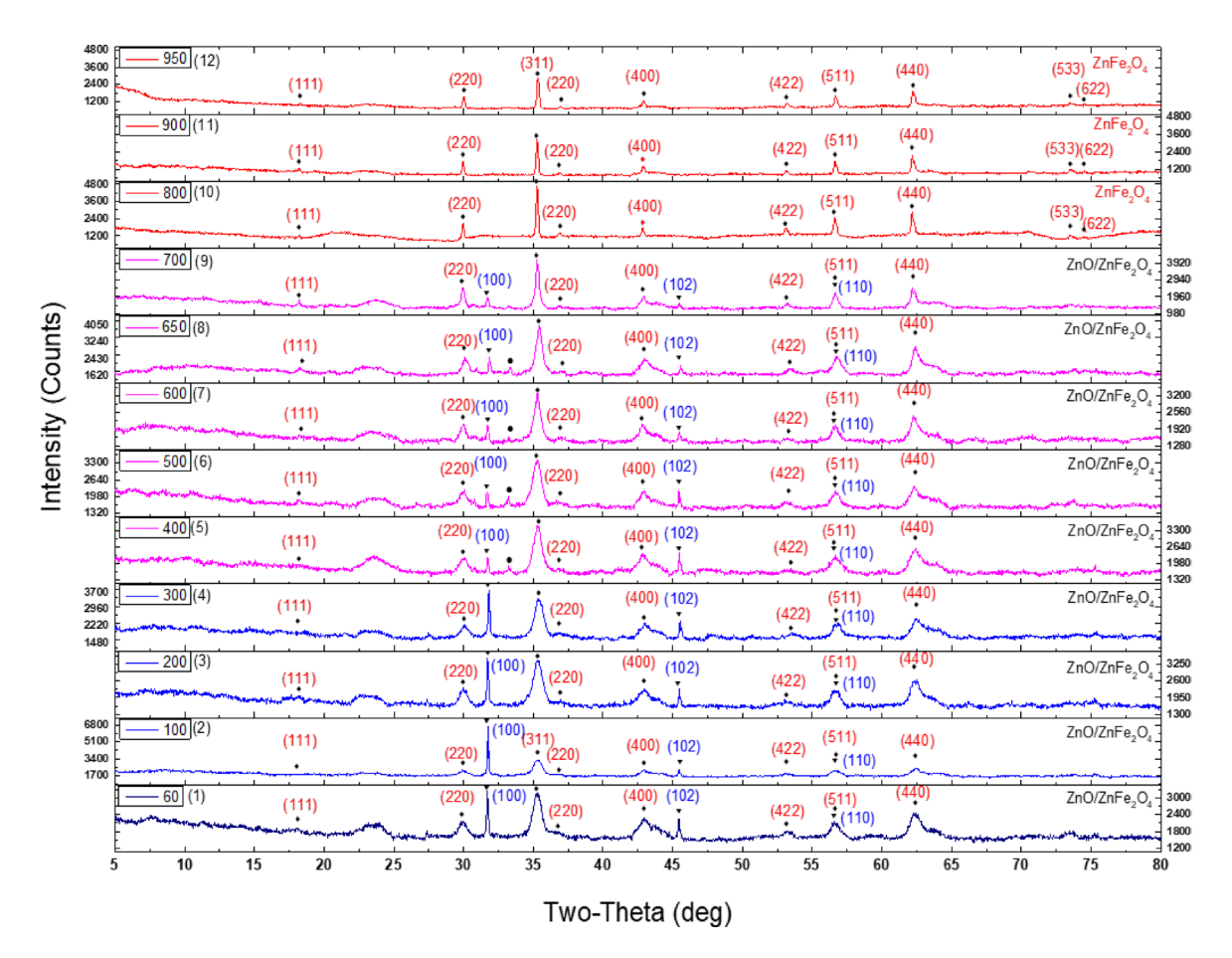


Fig. 1. XRD diagrams of samples of spinel-type nanosized Zn–Fe–O oxides were isothermally heated at (1) 60, (2) 100, (3) 200, (4) 300, (5) 400, (6) 500, (7) 600, (8) 650, (9) 700, (10) 800, (11) 900, and (12) 950 °C for 2 h.

(422), (511), (440), (531), (620), (533), (622), and (444), respectively are shown. The unnecessary minor lines can be ignored in XRD data and analysis. The appearance and disappearance of the lines located at $2\theta = 31.8^{\circ}$, d = 2.8135 Å, and I = 1682 counts were observed in the temperature range of 400–650 °C. It should be noted that XRD data and results of the as-prepared samples of the nanosized ZnO phase coincide with the standard pattern of PDF#74-0534, which contains with 11 lines (Zinc oxide, ZnO, Hexagonal, P63mc(186)). This phase exhibited the crystal parameters of 2θ (°) (31.768, 34.421, 47.538, 56.594, 66.374, 67.946, 72.566, and 76.958, respectively), d(Å) (2.8145, 2.6033, 1.9111, 1.6249, 1.4072, 1.3785, 1.3017, and 1.2379, respectively), I(%) (100, 19.8, 55.5, 22.9, 13.8, 19.4, 1.5, and 13.2, respectively), and (hkl), i.e. Miller index ((100), (002), (102), (110), (200), (112), (004), and (202), respectively). Therefore, the crystal phases of nanosized ZnO show the cubic structure in a cell (a, b, c (Å): 3.24986, 3.24986, 5.20662; α , β , γ (°): 90.0, 90.0, 120.0). It is evidenced that there was a significant change of a mixed structure of mixed ZnO-ZnFe,O4 converted into a single ZnFe,O4 structure in the range of annealing temperatures of 700-800 °C, which was due to the good incorporation of Zn into the ZnFe₂O₄ lattice. In the most important range of annealing temperatures of 800-950 °C, which was critical for the magnetic powder samples annealed for 2 h, the final products were nanosized $ZnFe_2O_4$ oxides formed in a single $ZnFe_2O_4$ phase, consistent with the standard of their crystallization (Franklinite, syn, cubic structure, Fd-3 m(227)). In the present research, the crystal phases and structures of large nanosized ZnFe₂O₄ oxide particles were formed by isothermally heated processes from 800, 900, and 950 °C for 2 h, respectively. The Scherrer equation $D = K \times \lambda /$ (FWHM×Cosθ) for one single crystal phase was used to estimate the crystallite sizes of Zn-Fe-O samples based on XRD data. K is the shape factor of the average crystallite (K = 0.89 - 0.94, typically taken as 0.9; $\lambda = 1.5406$ Å). The FWHM (Full Width at Half Maximum) was calculated at specific 2θ angles. The obtained values D, and D, of crystallite sizes of ZnO/ZnFe₂O₄ heated from 60 to 700 °C, and those of ZnFe₂O₄ (D₁) heated from 800 to 950 °C were listed in Table 1 using pattern simulation with pseudo-Voigt function.

The crystallite sizes of ZnFe₂O₄ (D₁) were determined to be 11 nm (60 °C), 10 nm (100 °C), 11 nm (200 °C), 12 nm (300 °C), 12 nm (400 °C), 12 nm (500 °C), 16 nm (600 °C), 15 nm (650 °C), 26 nm (700 °C), 63 nm (800 °C), 61 nm (900 °C), and 52 nm (950 °C), respectively. In hybrid ZnO/ZnFe₂O₄ samples heated in a range of 60–700 °C, the crystallite sizes of ZnO (D₂) were calculated to be 69 nm (60 °C), 75 nm (100 °C), 67 nm (200 °C), 55 nm (300 °C), 85 nm (400 °C), 56 nm (500 °C), 44 nm (600 °C), 48 nm (650 °C), and 23 nm (700 °C), respectively.

Samples	Temp. (°C)	Structure	D ₁ (nm)	D ₂ (nm)
1	60	ZnO/ZnFe ₂ O ₄	11.0 nm	69.0 nm
2	100	ZnO/ZnFe ₂ O ₄	10.0 nm	75.0 nm
3	200	ZnO/ZnFe ₂ O ₄	11.0 nm	67.0 nm
4	300	ZnO/ZnFe ₂ O ₄	12.0 nm	55.0 nm
5	400	ZnO/ZnFe ₂ O ₄	14.0 nm	85.0 nm
6	500	ZnO/ZnFe ₂ O ₄	12.0 nm	56.0 nm
7	600	ZnO/ZnFe ₂ O ₄	16.0 nm	44.0 nm
8	650	ZnO/ZnFe ₂ O ₄	15.0 nm	48.0 nm
9	700	ZnO/ZnFe ₂ O ₄	26.0 nm	23.0 nm
10	800	ZnFe ₂ O ₄	63.0 nm	0.0
11	900	ZnFe ₂ O ₄	61.0 nm	0.0
12	950	ZnFe ₂ O ₄	52.0 nm	0.0

Table 1. The crystallite sizes of $ZnO/ZnFe_2O_4$ and $ZnFe_2O_4$.

VSM: zigzag paramagnetism of nanosized ZnFe₂O₄ oxides

It is confirmed that all the as-prepared samples of nanosized Zn-Fe-O oxides exhibit the typical paramagnetic properties of magnetization curves (Hc, Ms, Mr, and χ), and very small remanent magnetic properties observed during the measured hysteresis cycles (Figs. 2 and 3). Refer to online supplementary material: supplementary Figures: S9, S10, S11, S12, S13, S14, S15, S16, S17, S18, S19, S20, S21, and S22 as well as S37 to S48 (original data). Refer to online supplementary material: supplementary Figures from \$23 to \$34. As shown in Figs. 2 and 3, the key paramagnetic parameters have been identified in the hysteresis loops with the upward and downward parts in the change of magnetization M dependent on external magnetic field H. The coercive field shows the applied field at which M/H changes sign, which leads the averaged values of Hc. Here, Mr means remanent magnetization of M at H=0. Additionally, saturation M (Ms) is observed when H increases or changes sign. Figure 3 shows the VSM measurements of nanosized Zn-Fe-O oxides, and the typical samples of nanosized Zn-Fe-O oxides by the polyol process, and the samples isothermally heated at 60, 100, 200, 300, 400, 500, 600, and 700 °C. These samples consisted of nanosized mixed ZnO and ZnFe₂O₄ oxides in the two crystal phases, with the corresponding magnetic parameters given in Tables 1 and 2. Figures 2, 3 and 4 also shows the VSM measurements of nanosized Zn-Fe-O oxides by the polyol process, and the samples isothermally heated at 800, 900, and 950 °C for 2 h, which displayed the very special forms of nanosized $ZnFe_2O_4$ oxides in the only crystal phase and structure (Franklinite, syn, ZnFe,O₄, cubic structure, Fd-3 m(227)). There are the similar shapes of hysteresis loops of four samples (60, 100, $\tilde{200}$, and 300 °C), four samples (400, 500, 600, and 650 °C), one sample (700 °C), three samples (800, 900, and 950 °C) in the four similar stages of hysteresis, which are typically paramagnetic properties, which can be ideally estimated and allowed in order to study and investigate three samples isothermally heated at 800, 900, and 950 °C, measured in the different ranges, respectively. The experimental values of calculated magnetic susceptibility (χ ; χ =M/H or linear fit of M according to H) of the Zn-Fe-O nanomaterials fabricated in this present study are positive but very small values. They have they magnitudes of 10^{-4} or 10^{-5} , as calculated in Table 2. This is good agreement with other works [49,50], which could be due to the interesting super-exchange interaction for superparamagnetic/paramagnetic behaviour responsible for all the as-prepared samples, especially for one typical sample heated at 400 °C for 2 h because of a new line appeared around at $2\theta = 31.8^{\circ}$ in XRD data of crystal structure of hybrid ZnO/ZnFe₂O₄. It is suggested that quantum-mechanical calculations by density functional theory (DFT) for understanding the magnetic behaviour of $\rm ZnFe_2O_4$ with the most typical $\rm [ZnO_4]$ and $\rm [FeO_6]$ models in a normal spinel structure or strongly correlated hybrid magnetic materials 48,49 . These particular interactions need to be studied further. This led to Mr of sample heated at 400 °C exhibiting the highest value among the mentioned samples as well as $ZnFe_2O_4$ by other methods^{1,2}.

It is noted that very weak superparamagnetism of nanosized Zn–Fe–O oxide samples isothermally heated at 60, 100, 200, 300, 400, and 700 °C was transformed into specific paramagnetism of nanosized Zn–Fe–O samples isothermally heated at 500, 600, 650, 800, 900, and 950 °C, respectively. Therefore, the magnetic characteristics consist of confirmed superparamagnetic and paramagnetic types in hybrid ZnO/ZnFe₂O₄ oxides, and in ZnFe₂O₄ oxides.

It is experimentally evidenced that nanosized mixed ZnO-ZnFe $_2$ O $_4$ -type Zn-Fe-O oxides have small values of Ms, ranging from 3.737 to 7.259 emu/g (Table 2) in respect with samples isothermally heated at 60, 100, 200, 300, 400, 500, 600, and 700 °C for 2 h. Here, the results show that nanosized mixed ZnFe $_2$ O $_4$ -type Zn-Fe-O oxides have Ms from 1.399 to 1.89 emu/g for samples heated at 800, 900, and 950 °C, respectively. The important variation of structure from nanosized mixed ZnO-ZnFe $_2$ O $_4$ -type Zn-Fe-O oxides formed in a temperature range of 60–700 °C into ZnFe $_2$ O $_4$ was observed in a temperature range from 800, 900, and 950 °C, respectively.

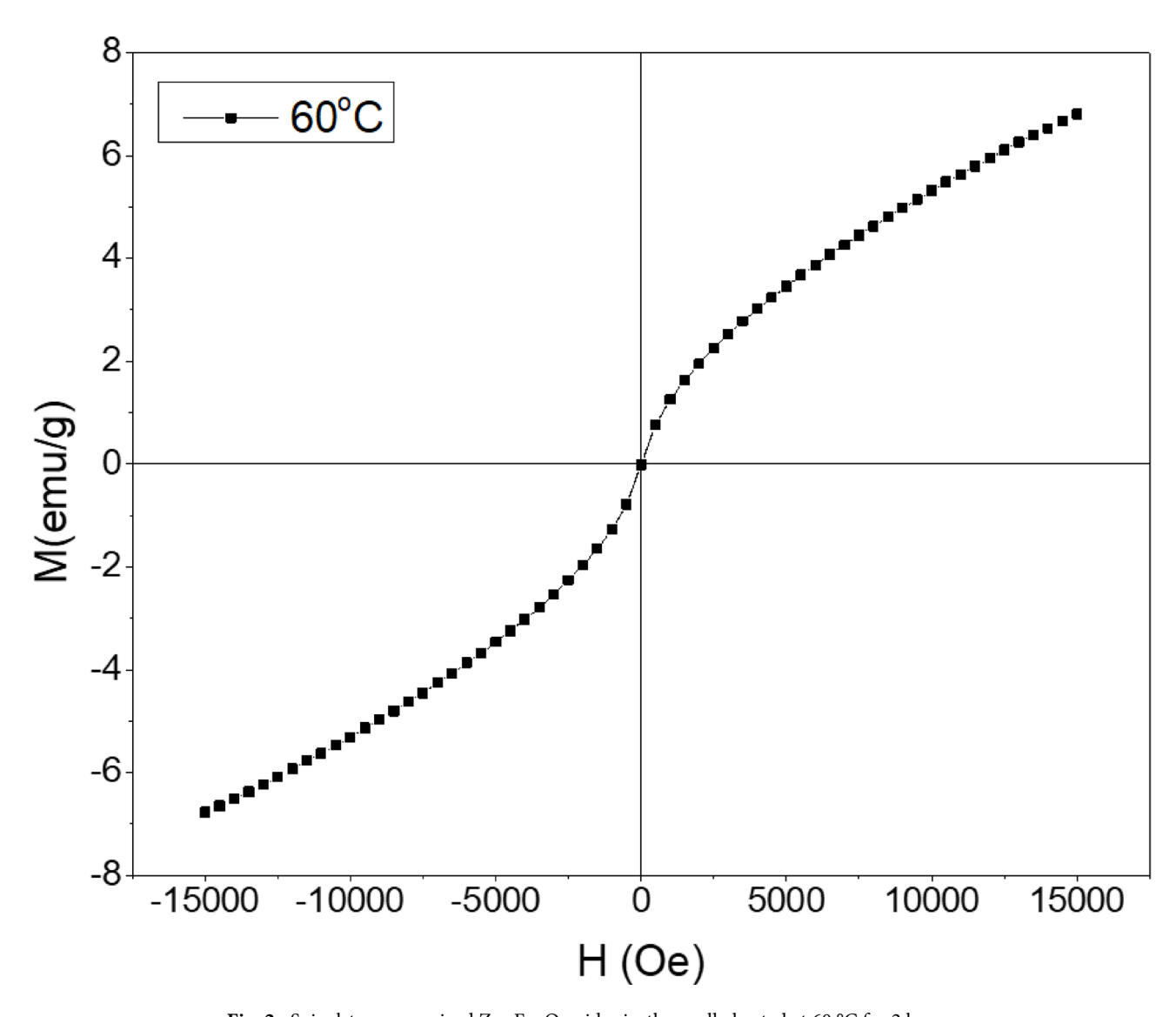


Fig. 2. Spinel-type nanosized Zn–Fe–O oxides isothermally heated at 60 °C for 2 h.

It is suggested that this led to the high stability of Zn^{2+} and Fe^{3+} cations at tetrahedral sites (T) and octahedral sites (O) in the theoretical defined crystal structure of $ZnFe_2O_4$ was relatively achieved through their balanced valences and cation distribution 30,31 .

It is observed that the variations of magnetic parameters of nanosized paramagnetic Zn–Fe–O oxide materials (Fig. 5) according to the calcination temperatures of the heat treatment process, including the average values of Hc, Mr, Ms, and χ as shown in Table 2, respectively. The values of Hc and Mr are relatively small in hysteresis loops. Mr tended to be proved in the up-part directions of hysteresis loops, which are negative values (-Mr) (see supplementary Figure S14). Here, ZnFe₂O₄ calcined at 800–950 °C for 2 h has high averaged value of Hc. The function of linear fit of M can be used in the case that is M=a+bH (emu/g) consistent with the mathematical estimation based on empirical data, meaning that the small value of M=b×H (emu/g) with a=0 and b=9.84×10⁻⁵ for a sample isothermally heated at 950 °C for a period of 2 h. Magnetic properties are related to each other, depending on the degree and nature of their structure and their interaction with external magnetic field³⁶. For magnetic nanomaterials, common types are ferromagnetic, ferrimagnetic, paramagnetic and superparamagnetic, diamagnetic, and ideal diamagnetic (superconducting). In nature, the magnetic properties of atoms or magnetic moment of atoms led different magnetic materials. One of the properties of magnetic ferri-, ferro-materials is that the degree of M depends complexly on H due to magnetic anisotropy and domains. However, paramagnetism and diamagnetism are approximately linearly proportional to H. To explain paramagnetism, researchers used classical Langevin theory or quantum theory of paramagnetism explained

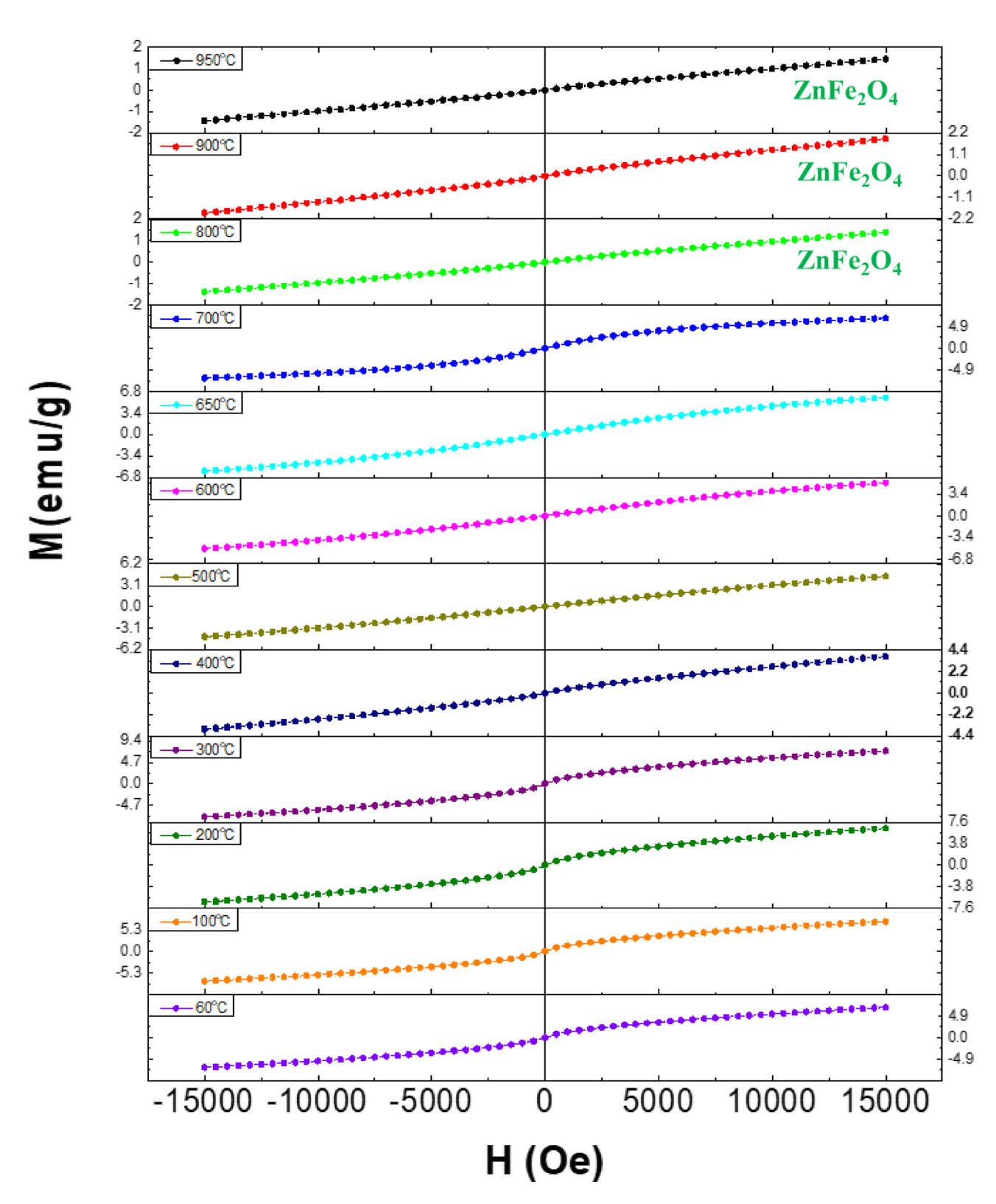


Fig. 3. Hysteresis loops of samples of spinel-type nanosized Zn–Fe–O oxides isothermally heated at (1) 60, (2) 100, (3) 200, (4) 300, (5) 400, (6) 500, (7) 600, (8) 650, (9) 700, (10) 800, (11) 900, and (12) 950 °C for 2 h.

Temp. (°C)	Hc (Oe)	Mr (emu/g)	Ms (emu/g)	x
60	5.985	0.0092993	6.799290	0.000519
100	4.925	0.0088498	7.259640	0.000558
200	4.829	0.0074320	6.527320	0.000497
300	4.831	0.0084485	7.249210	0.000557
400	0.021	0.4224227	3.737310	0.000265
500	0.023	0.0000083	4.392395	0.000305
600	0.027	0.0000123	5.171620	0.000374
650	0.025	0.0000139	5.813330	0.000430
700	0.021	0.0000238	6.797285	0.000545
800	62.525	0.0080471	1.399680	0.000097
900	22.752	0.0046301	1.896400	0.000132
950	50.028	0.0046268	1.438070	0.000098

Table 2. The averaged values of magnetic parameters of ZnO/ZnFe₂O₄ and ZnFe₂O₄.

by Brillouin functions when taking into account magnetic quantization,³⁷ which had clarified various kinds of nanosized ferrites ^{38,39}, as well as nanosized Fe-, Ni-, and Co-based ferrites as well as Ba- and Sr-based hexaferrites prepared by the polyol processes in experimental evidences and data²⁷. Here, ZnFe₂O₄ (or CdFe₂O₄) was a kind of normal-spinel ferrite with all Zn²⁺ (or Cd²⁺) cations at tetrahedral sites in the form of Zn²⁺[Fe₂, 3+]O₄ - that was different from inverse-spinel ferrite, i.e. M²⁺ cations stably located at octahedral sites (M: Co, Ni) in the form of $Fe^{3+}[M^{2+}Fe^{3+}]O_4^{\ 2-}$. It is suggested that the small contents of Zn element can change magnetic properties of $NiFe_2O_4$ or $CoFe_2O_4$ from ferrimagnetism into paramagnetism or superparamagnetism when Zn cations are well integrated into the inverse structures to form the various kinds of nanosized mixed spinel ferrites in the various mixed forms of $M^{2+}_{(1-x)}Fe_x^{3+}[M_x^{2+}Fe_{(2-x)}^{-3+}]O_4^{2-}$ ($0 \le x \le 1$), i.e. M^{2+} and Fe^{3+} possibly located in both tetrahedral sites and octahedral sites that leads the kinds of new high entropy ferrites³⁸. It is usually understood that the surveys of mixed normal and inverse spinel ferrites were identified in comparison with emphasizing and addressing the problems of magnetic structures and properties among them, ^{39,45} as well as other catalytic and electronic properties. In this case, it was believed that there is a complex dependence of M on H for the as-fabricated ZnFe₂O₄ materials (Fig. 4) from segments from (1) to (11) (See supplementary data file: Figures from \$23 to \$34). It is suggested that the magnetic phenomenon that there are many typical minor hysteresis loops (finely minor hysteresis loops) located on the main original loop of paramagnetic hysteresis. In typical paramagnetic behavior, the original paramagnetic hysteresis shows many short segments and lines, and other closed hysteresis loops of ZnFe₂O₄ that are paramagnetic and very small and weak ferromagnetic. In up and down parts of hysteresis, M-H loops appears the matching paramagnetic segments and lines (straight segments and lines (1a), 2(a), 9(a), 10(a), 11(a), and others), and extremely small ferromagnetic lines (closed curves), such as (2), (3), (4), (5), (6), (7), (8), (9), (10), and (11) belonging to original paramagnetic hysteresis of well-sintered nanosized ZnFe₂O₄ (Figs. 4 and 7). Similarly, it is noted that the segments and lines (3) and (10), (6) and (4) have the same shapes.

In terms of intrinsic property, the segments of original hysteresis correspond to paramagnetic phenomena (the zig-zag line: a segment and a line). In addition, very small ferromagnetism is observed on the original paramagnetic hysteresis. Such magnetic order requires further understanding and research. In our highlights, it is certain that the prepared samples also demonstrated that high paramagnetic nanosized ${\rm ZnFe_2O_4}$ oxides were finally heated and formed in the different stages of the crystal growth and stability through annealing and sintering.

SEM: nanosized ZnFe,O,

Typically, Figs. 6 and 7 show the interesting SEM and SEM/ EDX results of nanosized Zn–Fe–O oxide particles isothermally heated at 60 °C in the initial stage for ZnO/ZnFe₂O₄, and 950 °C for 2 h in the end stage for ZnFe₂O₄, which are novel nanosized structures. See supplementary data file: Figures S35 and S36.

It is evidenced that the issues of size, shape, and morphology of nanosized Zn-Fe-O oxide particles are studied when heated at 60 and 950 °C for 2 h. In these cases, the kinds of new, large, and special micro/nanotextures of magnetic ZnO/ZnFe₂O₄ particles (sample isothermally heated at 60 °C), and ZnFe₂O₄ oxide particles (sample isothermally heated at 950 °C, respectively) were adequately formed in the evolution from self-assembly of magnetic nanosized oxide particles or nanotextured particles by heat treatment at low and high temperatures. Furthermore, the role of shape-oriented nanoparticles in magnetic properties demonstrated in nanotextured ZnFe₂O₄ particles by various heat treatment processes. Finally, it is clear that elements were

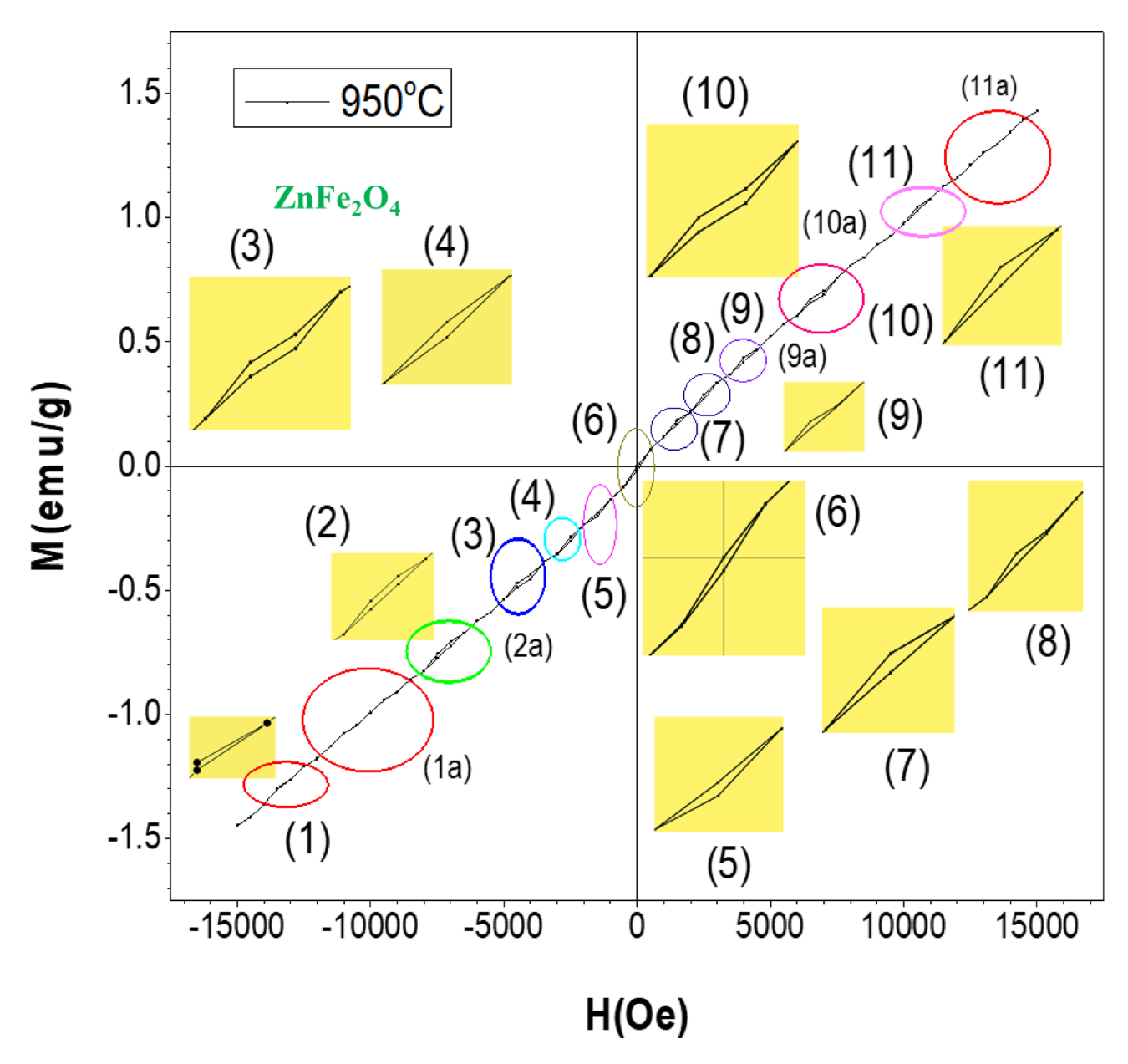


Fig. 4. Spinel-type nanosized Zn–Fe–O oxides isothermally heated at about 950 °C for 2 h. The phenomena of partitial hysteresis (closed curves) and linear hysteresis (linear segments) of down and up magnetization process.

experimentally found in SEM/EDX data and results for two samples sintered at 60 °C and 950 °C as shown in Figs. 6 and 7 including Fe(L), O(K), and Zn(L), respectively.

In this comparison, the evidence of elements (Fe, Zn, and O) is in agreement with the XRD measurements addressing the crystal phase formation of $\rm ZnFe_2O_4$ in two samples isothermally heated at 60 °C and 950 °C for 2 h. Figure 7a,b,c, and e show the large nanosized textures of $\rm ZnFe_2O_4$ particles, consisting of numerous small $\rm ZnFe_2O_4$ particles assembled together. Figure 7a,b,c,d, and e typically show polyhedral $\rm ZnFe_2O_4$ particles with very high and stable crystallinity. Specifically, this indicates a successful synthesis of nanosized spinel-type $\rm ZnFe_2O_4$ and other ferrites with desirable shapes and morphology^{40–48}. To enable further investigation, conventional ultrasonic sources, without the use of lasers, may be employed to disintegrate the nanosized particles. A diversity of sizes, shapes, and morphologies of nanosized spinel-type $\rm ZnFe_2O_4$ particles was observed. These particles exhibited a wide range of paramagnetic nanosized complex architectures, as revealed by our XRD and VSM results. Recently, nanosized $\rm ZnFe_2O_4$ has been used as a promising anode material in advanced lithium-ion batteries 43,44 .

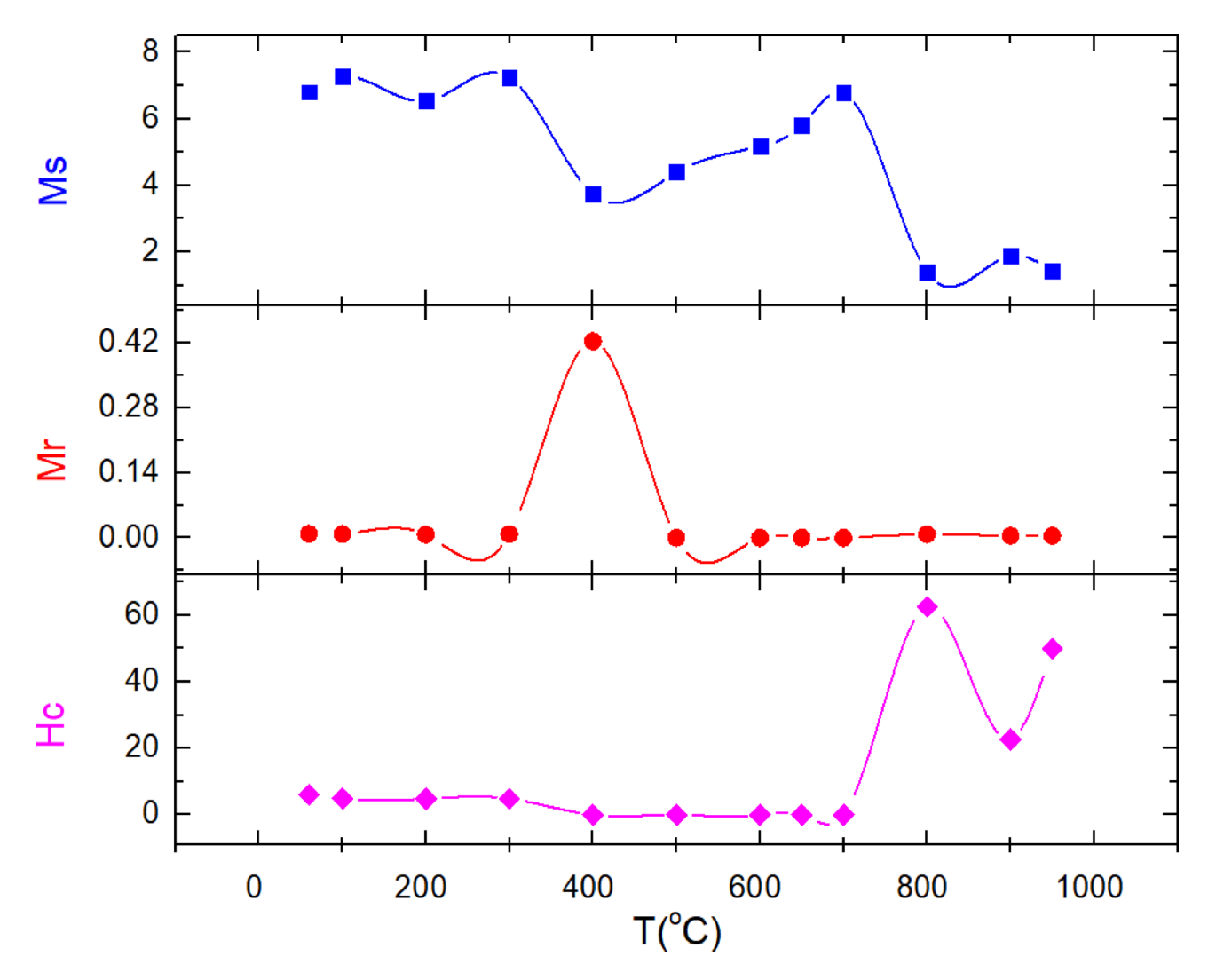


Fig. 5. Magnetic parameters of hysteresis loops of samples of spinel-type nanosized Zn–Fe–O oxides isothermally heated at about (1) 60, (2) 100, (3) 200, (4) 300, (5) 400, (6) 500, (7) 600, (8) 650, (9) 700, (10) 800, (11) 900, and (12) 950 °C for 2 h.

Conclusion

In this work, the paramagnetic properties of nanosized Zn–Fe–O oxides, including ZnO/ZnFe $_2$ O $_4$ and ZnFe $_2$ O $_4$, were studied in relation to their magnetic crystal structures. The effects of temperature and synthesis conditions on the paramagnetic behavior of these oxides were confirmed, particularly for nanosized ZnFe $_2$ O $_4$ ferrites subjected to isothermal heat treatment at 800, 900, and 950 °C for 2 h in the stability of micro/nanoscale structures. A distinctive zigzag magnetic behavior was observed during the synthesis of ZnFe $_2$ O $_4$. Several samples containing ZnFe $_2$ O $_4$ were prepared, each undergoing different polyol and heat treatment conditions, allowing for a comprehensive comparison of their magnetic properties. The polyol and heat treatment processes were optimized through systematic experimentation, where variables such as temperature, reaction time, and precursor concentrations were adjusted to achieve optimal nanosized textures and enhanced paramagnetic properties. These findings suggest that the optimized polyol synthesis and heat treatment techniques can be effectively applied for the production of high-entropy ferrites based on Co, Fe, and Ni, as well as Ba- and Sr-based hexaferrites.

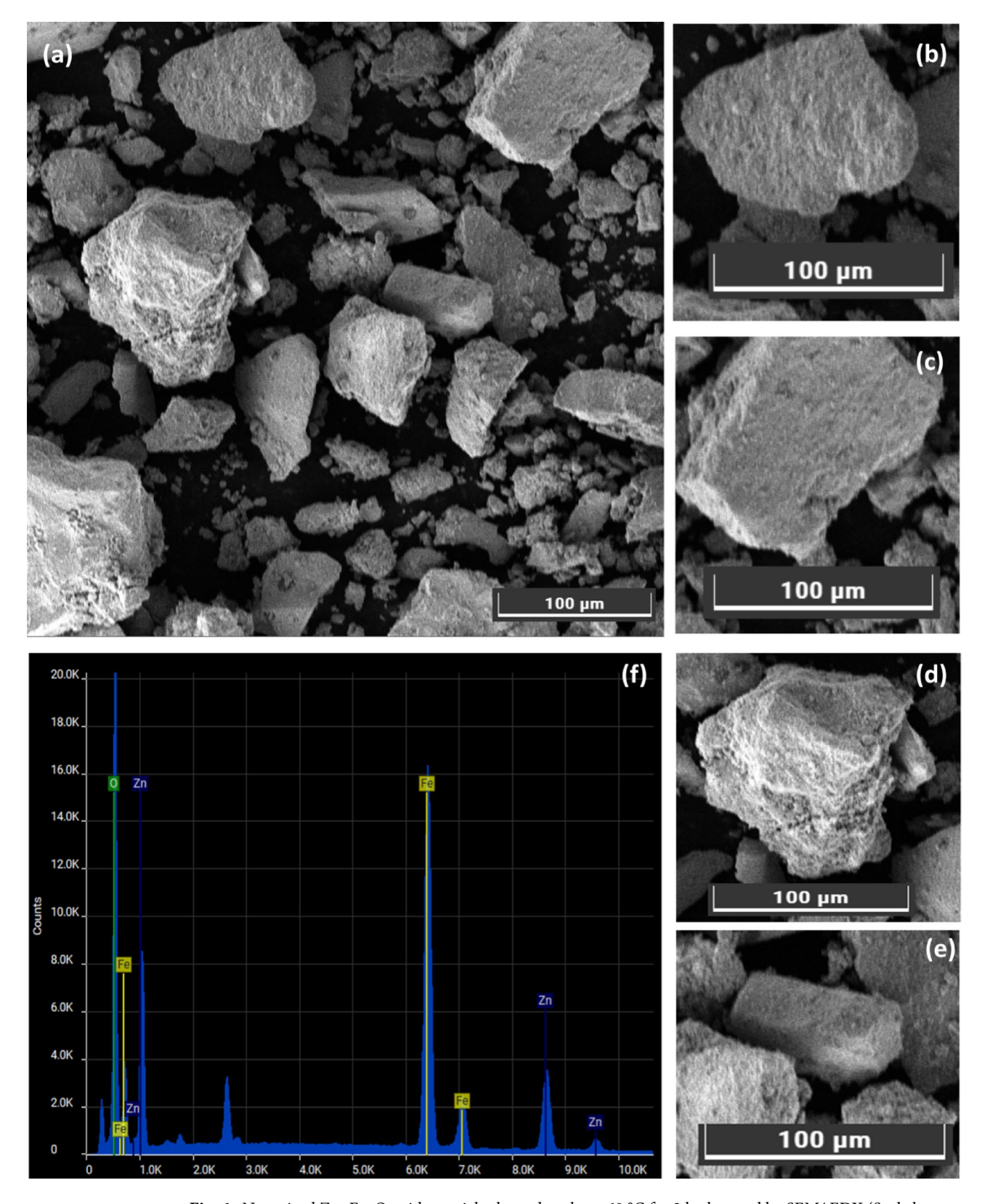


Fig. 6. Nanosized Zn–Fe–O oxide particles heated at about 60 °C for 2 h observed by SEM/ EDX (Scale bar: $100 \, \mu m$).

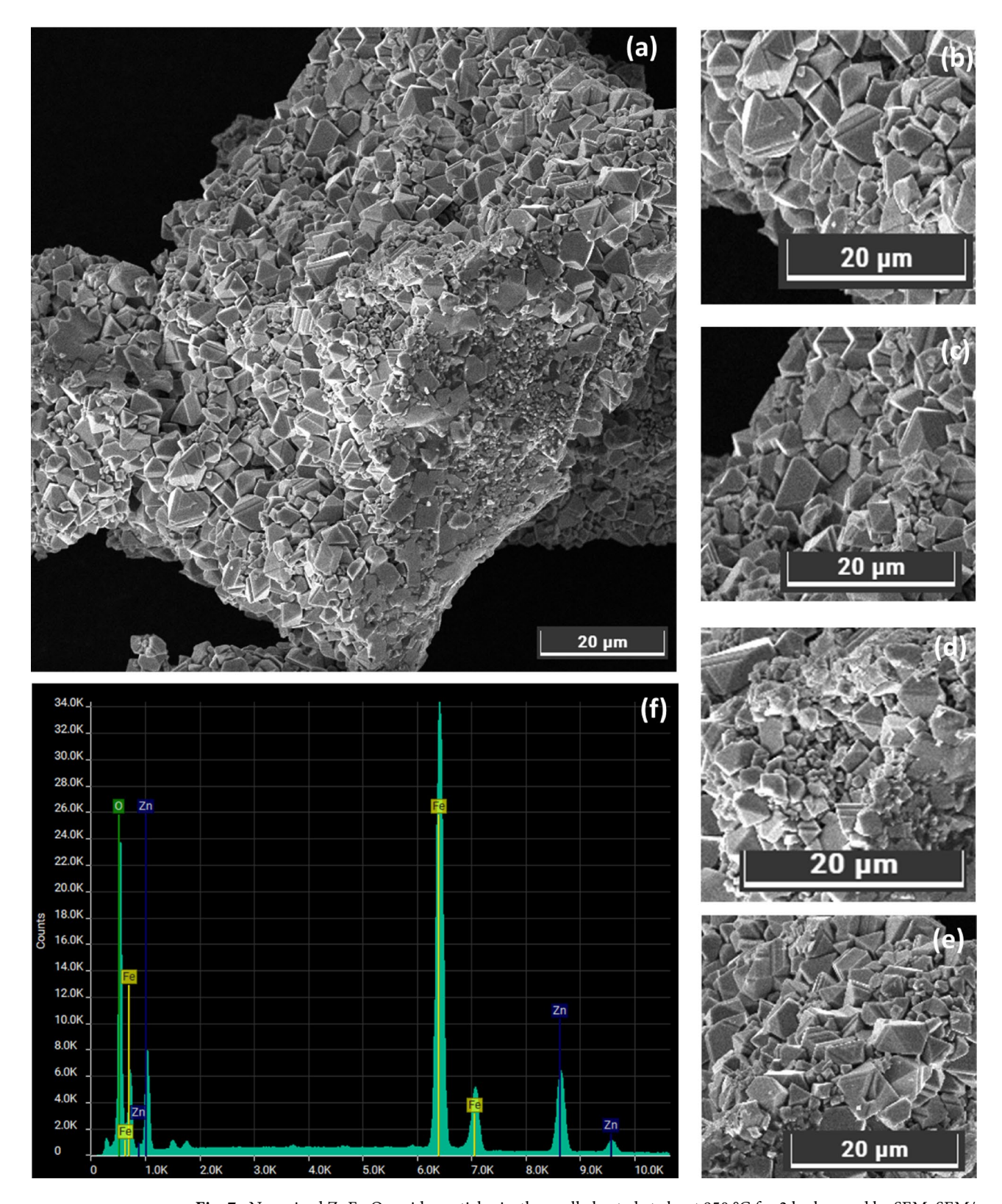


Fig. 7. Nanosized ZnFe $_2$ O $_4$ oxide particles isothermally heated at about 950 °C for 2 h observed by SEM, SEM/EDX methods (Scale bar: 20 μ m).

Data availability

Data will be available from the corresponding author upon request.

Received: 10 May 2025; Accepted: 10 September 2025

Published online: 13 October 2025

References

- 1. Yao, C. et al. ZnFe₂O₄ nanocrystals: Synthesis and magnetic properties. *J. Phys. Chem. C.* 111, 12274–12278. https://doi.org/10.10 21/jp0732763 (2007).
- Giri, J., Pradhan, P., Sriharsha, T. & Bahadur, D. Preparation and investigation of potentiality of different soft ferrites for hyperthermia applications. J. Appl. Phys. 15 (10). https://doi.org/10.1063/1.1855131 (2005).
- Hoque, S. M., Hossain, M. S., Choudhury, S., Akhter, S. & Hyder, F. Synthesis and characterization of ZnFe₂O₄ nanoparticles and its biomedical applications. *Mater. Lett.* 162, 60–63. https://doi.org/10.1016/j.matlet.2015.09.066 (2016).
- Antony, T. J. & Jagannathan, K. Structural, morphological and optical properties of ZnFe₂O₄-decorated reduced graphene oxide nanocomposite for antibacterial applications. Ceram. Int. 50, 16343–16351. https://doi.org/10.1016/j.ceramint.2024.02.116 (2024).
- Sandemann, J. R., Støckler, K. A. H., Wang, X., Chakoumakos, B. C. & Iversen, B. B. Benchmark crystal structure of defect-free spinel ZnFe₂O₄. J. Am. Chem. Soc. 145, 21053–21065. https://doi.org/10.1021/jacs.3c07334 (2023).
- Sai, R., Kulkarni, S. D., Vinoy, K. J., Bhat, N. & Shivashankar, S. A. ZnFe₂O₄: rapid and sub-100 °C synthesis and anneal-tuned magnetic properties. *J. Mater. Chem.* 22, 2149–2156. https://doi.org/10.1039/C1JM14874E (2012).
- Ajormal, F., Moradnia, F., Fardood, S. T. & Ramazani, A. Zinc ferrite nanoparticles in photo-degradation of dye: mini-review. J. Chem. Rev. 2, 90–102. https://doi.org/10.33945/SAMI/JCR.2020.2.2 (2020).
- Valenzuela, M. A., Bosch, P., Jiménez-Becerrill, J., Quiroz, O. & Páez, A. I. Preparation, characterization and photocatalytic activity of zno, Fe₂O₃ and ZnFe₂O₄. J. Photochem. Photobiol A: Chem. 148, 177–182. https://doi.org/10.1016/S1010-6030(02)00040-0 (2002)
- 9. Lemine, O. M. et al. Synthesis, structural, magnetic and optical properties of nanocrystalline ZnFe₂O₄. *Phys. B: Condens. Matter.* **406**, 1989–1994. https://doi.org/10.1016/j.physb.2011.02.072 (2011).
- Upadhyay, C., Verma, H. C., Sathe, V. & Pimpale, A. V. Effect of size and synthesis route on the magnetic properties of chemically prepared nanosize ZnFe₂O₄. J. Magn. Magn. Mater. 312, 271–279. https://doi.org/10.1016/j.jmmm.2006.10.448 (2007).
- Ding, Y., Yang, Y. & Shao, H. High capacity ZnFe₂O₄ anode material for lithium ion batteries. *Electrochim. Acta.* 56, 9433–9438. https://doi.org/10.1016/j.electacta.2011.08.031 (2011).
- Huang, M. et al. Heterogeneous interface engineering of Bi-Metal MOFs-derived ZnFe₂O₄–ZnO-Fe@C microspheres via confined growth strategy toward superior electromagnetic wave absorption. Adv. Funct. Mater. 34:2308898. (2024). https://doi.org/10.1002/adfm.202308898
- 13. Faramawy, A. M. & El-Sayed, H. M. Enhancement of magnetization and optical properties of CuFe₂O₄/ZnFe₂O₄ core/shell nanostructure. *Sci. Rep.* **14**, 6935. https://doi.org/10.1038/s41598-024-57134-7 (2024).
- 14. Lys, A. et al. Core-shell nanofibers of ZnFe₂O₄/ZnO for enhanced visible-light photoelectrochemical performance. *J. Alloys Compd.* 984, 173885. https://doi.org/10.1016/j.jailcom.2024.173885 (2024).
- 15. Tomar, D. & Jeevanandam, P. Synthesis of ZnFe₂O₄ nanoparticles with different morphologies via thermal decomposition approach and studies on their magnetic properties. *J. Magn. Magn. Mater.* **564**, 170033. https://doi.org/10.1016/j.jmmm.2022.170033 (2022).
- Renuka, L. et al. Synthesis of ZnFe₂O₄ nanoparticle by combustion and Sol gel methods and their structural, photoluminescence and photocatalytic performance. *Mater. Today Proc.* 5, 20819–20826. https://doi.org/10.1016/j.matpr.2018.06.467 (2018).
- Kumar, S. et al. Superparamagnetic dy modified ZnFe₂O₄ magnetic nanophotocatalysts for the photocatalytic degradation of crystal Violet pollutant. Appl. Phys. A. 130, 1–17. https://doi.org/10.1007/s00339-024-07431-9 (2024).
- Vergis, B. R., Kottam, N., Krishna, R. H. & Nagabhushana, B. M. Removal of Evans blue dye from aqueous solution using magnetic spinel ZnFe₂O₄ nanomaterial: adsorption isotherms and kinetics. *Nano-Struct Nano-Objects*. 18, 100290. https://doi.org/10.1016/j.nanoso.2019.100290 (2019).
- Qureashi, A. et al. ZnFe₂O₄ loaded on municipal waste-char: outstanding adsorption and photocatalytic removal of contaminants. New. J. Chem. 48, 8479–8494. https://doi.org/10.1039/D4NJ00604F (2024).
- Sarifuddin, W. S. et al. Cu doped ZnFe₂O₄ photocatalysts for enhanced hydrogen production and dye degradation in the visible region. J. Photochem. Photobiol A: Chem. 115658 https://doi.org/10.1016/j.jphotochem.2024.115658 (2024).
- 21. Feng, Y. et al. Enhanced photoelectric performance of ZnFe₂O₄ catalysts for oxidative carboxylation of styrene by tuning crystal planes and thermal and electrical conductivity. *J. Clean. Prod.* **440**, 141002. https://doi.org/10.1016/j.jclepro.2024.141002 (2024).
- Xie, Q., Huang, H., Zhang, C., Zheng, X. & Shi, H. Manipulating spin-polarization of Co-doped ZnFe₂O₄ for photocatalytic TC degradation. J. Phys. D: Appl. Phys. 57, 165104. https://doi.org/10.1088/1361-6463/ad2094 (2024).
- 23. Nisa, S. & Rana, A. M. Stable positive unipolar resistive switching in chemical solution-deposited nanocrystalline spinel ferrite ZnFe₂O₄. *Mod. Phys. Lett. B.* 2450284. https://doi.org/10.1142/S0217984924502841 (2024).
- Zaman, F. U. et al. Enhanced photocatalytic degradation of organic dyes by carbon quantum dots-ZnFe₂O₄ composites. J. Alloys Compd. 983, 173860. https://doi.org/10.1016/j.jallcom.2024.173860 (2024).
- Guo, H., Marschilok, A. C., Takeuchi, K. J., Takeuchi, E. S. & Liu, P. Essential role of spinel ZnFe₂O₄ surfaces during lithiation. ACS Appl. Mater. Interfaces. 10, 35623–35630. https://doi.org/10.1021/acsami.8b12869 (2018).
- 26. Fiévet, F. et al. The polyol process: a unique method for easy access to metal nanoparticles with tailored sizes, shapes and compositions. Chem. Soc. Rev. 47, 5187–5233. https://doi.org/10.1039/C7CS00777A (2018).
- Long, N. V., Hang, N. T. N. & Cuu, H. V. Micro/nanosized ferrite and hexaferrite structures: the polyol processes for synthesis. *Int. J. Nanomater Nanotechnol Nanomed.* 9, 024–026. https://doi.org/10.17352/2455-3492.000054 (2023).
- 28. Long, N. V., Hang, N. T. N., Yang, Y. & Nogami, M. Synthesis of Cobalt and Its Metallic Magnetic Nanoparticles. In: Thomas S, Rezazadeh N A (eds) Handbook of Magnetic Hybrid Nanoalloys and their Nanocomposites. Springer, Cham (2022). https://doi.org/10.1007/978-3-030-90948-2_5
- 29. Long, N. V. et al. The development of mixture, alloy, and core-shell nanocatalysts with nanomaterial supports for energy conversion in low-temperature fuel cells. *Nano Energy.* **2**, 636–676. https://doi.org/10.1016/j.nanoen.2013.06.001 (2013).
- Long, N. V. et al. Gas-sensing properties of p-type α-Fe₂O₃ polyhedral particles synthesized via a modified polyol method. RSC Adv. 4, 8250–8255. https://doi.org/10.1039/C3RA46410E (2014).
- Long, N. V. et al. Synthesis and magnetism of hierarchical iron oxide particles. Mater. Des. 86, 797–808. https://doi.org/10.1016/j.matdes.2015.07.157 (2015).
- 32. Busharat, M. A. et al. Study of cation distribution and photocatalytic activity of nonthermal Plasma-Modified NiZnFe₂O₄ magnetic nanocomposites. *ACS Omega.* **9**, 14791–14804. https://doi.org/10.1021/acsomega.3c06883 (2024).
- 33. Yuan, Q. et al. SnO₂ QDs sensitized ZnFe₂O₄ spheres with enhanced acetone sensing performance. *Nanotechnol* 35, 275502. https://doi.org/10.1088/1361-6528/ad39f3 (2024).
- 34. Bresser, D. et al. Carbon coated ZnFe₂O₄ nanoparticles for advanced lithium-ion anodes. *Adv. Energy Mater.* **3**, 513–523. https://doi.org/10.1002/aenm.201200735 (2013).

- 35. Zhao, Q., Yan, Z., Chen, C. & Chen, J. Spinels: controlled preparation, oxygen reduction/evolution reaction application, and beyond. *Chem. Rev.* 117, 10121–10211. https://doi.org/10.1021/acs.chemrev.7b00051 (2017).
- 36. Kittel, C. Introduction to Solid State Physics, 8th ed., Wiley, 703 pages. Chapter 11 (p. 297), and Chap. 12 (p. 321) (2005).
- 37. Andersen, H. L., Granados-Miralles, C., Jensen, K. M., Saura-Múzquiz, M. & Christensen, M. The chemistry of spinel ferrite nanoparticle nucleation, crystallization, and growth. ACS Nano. 18, 9852–9870. https://doi.org/10.1021/acsnano.3c08772 (2024).
- 38. Zander, J. et al. Medium-and High-Entropy spinel ferrite nanoparticles via low-temperature synthesis for the oxygen evolution reaction. *Adv. Funct. Mater.* **34**, 2310179. https://doi.org/10.1002/adfm.202310179 (2024).
- 39. Zhu, K. et al. Magnetic nanomaterials: chemical design, synthesis, and potential applications. *Acc. Chem. Res.* 51, 404–413. https://doi.org/10.1016/j.foodchem.2023.137061 (2018).
- Elmore, W. C. Ferromagnetic colloid for studying magnetic structure. Phys. Rev. 54, 309–310. https://doi.org/10.1103/PhysRev.54.309 (1938).
- 41. Welo, L. A. & Baudisch, O. LXII. Ferromagnetism in the oxide obtained by dehydration of gamma ferric oxide hydrate. *Lond. Edinb. Dublin Philosophical Magazine J. Sci.* 17, 753–768. https://doi.org/10.1080/14786443409462432 (1934).
- 42. Ding, Y., Yang, Y. & Shao, H. High capacity ZnFe₂O₄ anode material for lithium ion batteries. *Electrochim. Acta.* **56**, 9433–9438. https://doi.org/10.1016/j.electacta.2011.08.031 (2011).
- 43. Martinez-Julian, F. et al. Probing lithiation kinetics of carbon-coated ZnFe₂O₄ nanoparticle battery anodes. *J. Phys. Chem. C.* 118, 6069–6076. https://doi.org/10.1021/jp412641v (2014).
- 44. Tatarchuk, T. R., Bououdina, M., Paliychuk, N. D., Yaremiy, I. P. & Moklyak, V. V. Structural characterization and antistructure modeling of cobalt-substituted zinc ferrites. J. Alloys Compd. 694, 777–791. https://doi.org/10.1016/j.jallcom.2016.10.067 (2016).
- 45. Long, N. V., Yang, Y., Thi, C. M., Phuc, L. H. & Nogami, M. Controlled synthesis and ferrimagnetism of homogeneous hierarchical CoFe, O_A particles. *J. Electron. Mater.* 46, 6001–6008. https://doi.org/10.1007/s11664-017-5568-8 (2016).
- 46. Long, N. V., Yang, Y., Thi, C. M., Phuc, L. H. & Nogami, M. Controlled synthesis and magnetic properties of uniform hierarchical polyhedral α-Fe₂O₃ particles. *J. Electron. Mater.* **46**, 3301–3308. https://doi.org/10.1007/s11664-017-5360-9 (2016).
- 47. Nguyen, M. D. et al. Nickel-Zinc ferrite nanoparticles for hyperthermia: Preserving superparamagnetism across a broad range of particle sizes. ACS Appl. Mater. Interfaces. 17, 22929–22940. https://doi.org/10.1021/acsami.5c00830 (2025).
- 48. Oliveira De, R. C. et al. Role of surfaces in the magnetic and Ozone gas-sensing properties of ZnFe₂O₄ nanoparticles: Theoretical and experimental insights. ACS Appl. Mater. Interfaces. 13 (3), 4605–4617. https://doi.org/10.1021/acsami.0c15681 (2021).
- Rezende, A. F. et al. DFT calculations for structural, electronic, and magnetic properties of ZnFe₂O₄ spinel oxide: The role of exchange-correlation functional. *Mater. Res.* 25, e20220219. https://doi.org/10.1590/1980-5373-MR-2022-0219 (2022).

Acknowledgements

This research is funded by Vietnam National Foundation for Science and Technology Development (NAFOST-ED) under grant number 103.02-2021.32.

Author contributions

Nguyen Viet Long conducted the experiments, collected the data and results, wrote the entire original manuscript, and evaluated and discussed the results and insights into the polyol processes for synthesis of micro/nanosized iron oxides, ferrites and hexaferrites oxides. Nguyen Thi Nhat Hang, Yong Yang, Le Hong Phuc, Nguyen Quan Hien, Ho Van Cuu, Nguyen Huu Tri, Nguyen Xuan Hoang, Masayuki Nogami, and Nguyen Viet Long reviewed and discussed experimental data and research results. All the authors have read and agreed to the published version of the manuscript. This study is original and novel experimental study that complements the theory and experiment of magnetization, demagnetization field, zigzag paramagnetism of nanosized $\rm ZnFe_2O_4$ oxides. This manuscript is the authors' original work and has not been published nor has it been submitted simultaneously elsewhere. All authors have checked the manuscript and have agreed to the submission.

Funding

Open access funding provided by Vietnam National Foundation for Science and Technology Development (NAFOSTED). This research is funded by Vietnam National Foundation for Science and Technology Development (NAFOSTED) under grant number 103.02-2021.32.

Declarations

Competing interests

On behalf of all authors, the corresponding author states that there is no conflict of interest.

Ethical approval

The data presented in our research do not involve animal or human health data as well as human tissue engineering.

Additional information

Supplementary Information The online version contains supplementary material available at https://doi.org/1 0.1038/s41598-025-19772-3.

Correspondence and requests for materials should be addressed to N.V.L.

Reprints and permissions information is available at www.nature.com/reprints.

Publisher's note Springer Nature remains neutral with regard to jurisdictional claims in published maps and institutional affiliations.

Open Access This article is licensed under a Creative Commons Attribution-NonCommercial-NoDerivatives 4.0 International License, which permits any non-commercial use, sharing, distribution and reproduction in any medium or format, as long as you give appropriate credit to the original author(s) and the source, provide a link to the Creative Commons licence, and indicate if you modified the licensed material. You do not have permission under this licence to share adapted material derived from this article or parts of it. The images or other third party material in this article are included in the article's Creative Commons licence, unless indicated otherwise in a credit line to the material. If material is not included in the article's Creative Commons licence and your intended use is not permitted by statutory regulation or exceeds the permitted use, you will need to obtain permission directly from the copyright holder. To view a copy of this licence, visit http://creativecommons.org/licenses/by-nc-nd/4.0/.

© The Author(s) 2025